Journal of The Electrochemical Society, **152** (7) A1452-A1457 (2005)
0013-4651/2005/152(7)/A1452/6/$7.00 © The Electrochemical Society, Inc.

Sn-Carbon Core-Shell Powder for Anode in Lithium Secondary Batteries

Yoon Seok Jung,[a] Kyu T. Lee,[a] Ji Heon Ryu,[a] Dongmin Im,[b] and Seung M. Oh[a,*,z]

[a]*School of Chemical and Biological Engineering, and Research Center for Energy Conversion and Storage, Seoul National University, Seoul 151-742, Korea*
[b]*Materials Laboratroy, Samsung Advanced Institute of Technology, Suwon, 440-600, Korea*

Spherical Sn-carbon core-shell powder was synthesized through a resorcinol-formaldehyde (RF) microemulsion polymerization performed in the presence of hydrophobized Sn nanoparticles. The Sn-carbon core-shell structure was found to greatly enhance the cycle life compared to the mixture of Sn and spherical carbon when evaluated as the anode in lithium-ion batteries. A core-shell powder containing 20 wt % Sn showed 69% capacity retention at the 40th cycle when cycled between 0 and 2.0 V (vs Li/Li^+) at a constant current of 40 mA g^{-1}. The mixture of 20 wt % Sn nanopowder and 80 wt % spherical carbon powder exhibited only 10% capacity retention in the same test condition. It is believed that the improved cyclability achieved with the core-shell powder is largely attributed to the inhibition of aggregation between Sn nanoparticles. The marginal polarization due to an intimate electrical contact made between Sn core and carbon shell is an additional advantageous feature achieved with this electrode.
 [DOI: 10.1149/1.1933616]

Manuscript received February 15, 2005. Available electronically June 16, 2005.

Metallic Sn has attracted much interest as one of the promising alternatives to the carbon-based anode for lithium secondary batteries. Its theoretical specific capacity (992 mAh g^{-1}) is much higher than that of already-commercialized graphite (372 mAh g^{-1}).[1-3] One of the critical problems encountered with this anode is, however, the severe volume change during the alloying and dealloying reaction with Li^+ ions. Due to the repeated volume change upon cycling, Sn particles are pulverized to lose their Li^+ storage ability.[4] It has been reported that pulverization can be alleviated by reducing the particle size of lithium host phase, fabricating nanocomposites of intermetallics, and using barrier materials.[5-15] Even with these nanosized materials, however, another problem still remains in that small metal particles are aggregated to be larger ones during the alloying and dealloying period, then pulverized again.[6,16,17]

One of our approaches to improve the cycle life of nanosized Sn particles is to encapsulate them with spherical carbon.[14] The carbon shell is envisaged to play several important roles in this preparation. First it acts as a barrier to inhibit the aggregation of nanosized Sn particles by minimizing the direct contact points between them. Second, the electrical contact between Sn core and carbon shell would be maintained even if the Sn particles were cracked or pulverized inside the carbon shell. Finally, the carbon shell itself reversibly reacts with Li^+ ions to deliver additional Li^+ storage capacity.

In this work, we have successfully prepared the Sn-carbon core-shell structure using a resorcinol-formaldehyde (RF) microemulsion polymerization technique. The electrochemical performances of this core-shell powder for anode in lithium-ion batteries are presented. Microstructural analyses have also been made and the relationship between the morphological change and electrochemical response is discussed.

Experimental

Preparation of Sn-carbon core-shell powder.— The synthetic procedure is summarized in Scheme 1. The key feature in this preparation is the hydrophobization of Sn nanoparticles and the formation of core-shell structured Sn-RF sol that is further stabilized by surfactants in aqueous medium. In detail, resorcinol (R, 4 mmol), formaldehyde (F, 4 mol, 300 mL of 37 wt % aqueous solution), sodium carbonate (0.075 mmol as a catalyst), and cetyltrimethylammonium bromide (CTAB, 0.988 mmol as a surfactant) were dispersed in deionized water (200 mL) to form RF microemulsion. Hydrophobized Sn nanoparticles were separately prepared by first dispersing the Sn nanoparticles (Alfa Aesar) in ethanol containing *1*-octadecanethiol (5% of Sn by weight) and then evaporating the solvent. For the formation of core-shell structured Sn-RF sol, the hydrophobized Sn nanoparticles (200 mg) were added into the RF microemulsion, and dispersed by sonication and vigorous stirring. For the polymerization of RF sol, the mixture was heated at 85°C for 3 days, which was followed by drying at the same temperature. The resulting Sn-RF gel was heat treated at 1000°C for 1 h under argon atmosphere to carbonize the RF gel. During this period, the Sn particles located inside the carbon shell are melted upon heating and solidified again after cooling.

Material characterization.— Microscopic investigation was carried out with a JEOL JEM 2000 EXII transmission electron microscope (TEM) and a JSM 6700F field-emission scanning electron microscope (FE-SEM). In addition to the as-prepared sample, the core-shell Sn-carbon particles after cycling were also analyzed with TEM, for which the electrode was rinsed with dimethyl carbonate (DMC) in a glove box, dried under vacuum, and sonicated to disperse the particles in absolute ethanol. X-ray diffraction (XRD) patterns were recorded using a Bruker D8 Advance with Cu $K\alpha$ radiation at a scan rate of 3.75 deg/min^{-1}. The Sn content was determined from the thermogravimetric analysis (TGA) profile that was obtained from room temperature to 1000°C at 20°C min^{-1} in air with a TA instrument Q600 simultaneous DSC/TGA analyzer. Because only SnO_2 would remain after all the organic components being oxidized into gaseous CO_2 and H_2O after TGA experiment, the Sn content could be calculated based on the initial and final weight of sample as represented in Eq. 1

$$\text{Sn content}(\%) = 100 \times \frac{\text{molecular weight of Sn}}{\text{molecular weight of } SnO_2} \times \frac{\text{final weight}}{\text{initial weight}} \quad [1]$$

Electrochemical characterization.— A beaker-type three-electrode cell was employed to assess the electrochemical performance of samples. Lithium foils (Cyprus Co.) were used as the counter and reference electrode, and 1.0 M $LiClO_4$ dissolved in a mixture of ethylene carbonate (EC) and diethyl carbonate (DEC) (1:1, v/v) was used as the electrolyte. The composite electrodes were prepared by spreading a mixture of core-shell powder, Super P (carbon additive for conductivity enhancement) and polytetrafluoroethylene (PTFE as a binder) (10:1:1 weight ratio) on a piece of copper exmet (as a current collector, apparent area = 1 cm^2). The electrodes were then dried at 120°C under vacuum for 12 h and subsequently pressed in order to enhance the interparticle contact and to ensure a better adhesion to the current collector.

* Electrochemical Society Active Member.
z E-mail: seungoh@plaza.snu.ac.kr

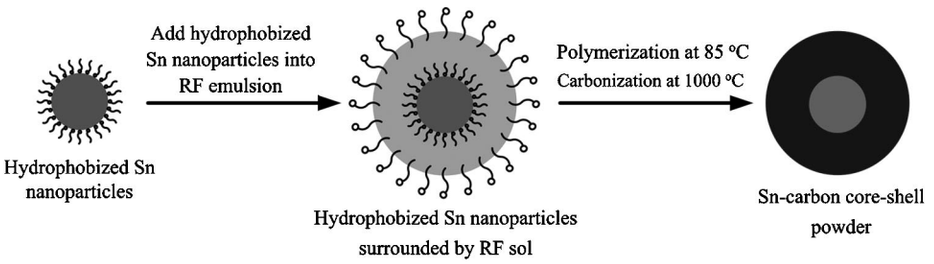

Scheme 1. Schematic diagram for the synthesis of Sn-carbon core-shell powder.

Galvanostatic charge-discharge cycling was made with a current density of 40 mA g^{-1} in the voltage range 0 to 2.0 V (vs Li^+/Li). The galvanostatic intermittent titration technique (GITT) was employed to monitor the evolution of electrode polarization during cycling, where a current pulse of 40 mA g^{-1} was applied for 5 min to measure the closed-circuit voltage (CCV) and turned off for 20 min to obtain the quasi-open-circuit voltage (QOCV). The sequential current pulse was applied for both charging and discharging period in the range of 0-2.0 V (vs Li/Li^+). Polarization value was calculated from the difference between the CCV and QOCV in each voltage transient. All the electrochemical experiments were conducted at 25°C in a glove box.

Results and Discussion

Characterization of Sn-carbon core-shell powder.— A TEM image of hydrophobized Sn nanoparticles is shown in Fig. 1. The shape is spherical and the size is typically in the range 100 to 300 nm. Because only the particles having sufficiently hydrophobic surface can be encapsulated by RF sol, the surface of Sn nanoparticles was hydrophobized with 1-octadecanethiol. The thiol functional group in this molecule is very likely adsorbed on the surface of Sn with the alkyl chain directing outside. The hydrophobic nature can be confirmed by their preference for nonpolar solvents as manifested in Fig. 2. It is seen that the thiol-treated Sn nanoparticles (Fig. 2b) are readily extracted to the hydrophobic *n*-hexane layer (upper) from the hydrophilic aqueous layer (lower), whereas the bare Sn nanoparticles are not (Fig. 2a).

Once hydrophobized Sn nanoparticles are added into the RF emulsion, as they are more hydrophobic than RF sol, the Sn particles are supposed to place at the innermost region (core), and the RF sol at the outside (shell).[18,19] The FE-SEM and TEM images of Sn-carbon core-shell powder that was obtained after polymerization and carbonization are presented in Fig. 3a and b, respectively. The particles are spherical in shape and uniform in size (Fig. 3a). It is seen in Fig. 3b that the size and shape of Sn nanoparticles (the darker image in the core) do not change significantly, although they apparently experience a liquid state during the heat treatment. Note that the melting point of Sn is 231.9°C. Carbon shell thus appears to keep liquid Sn in the core from leaching out even at high temperature (1000°C). This Sn-carbon core-shell structure would minimize the particle aggregation because the direct contact between Sn particles is negligible.

Figure 4 shows the XRD pattern of a Sn-carbon core-shell powder. All the peaks can be assigned to those of β-Sn (JCPDS no. 04-0673). Peaks corresponding to any oxide phases are not found, implying that any Sn-oxide compounds on the surface of Sn nanoparticles have been reduced to metallic Sn by carbothermal reduction. In addition, the absence of peaks corresponding to graphite and the presence of a broad peak at 23° indicates that the resulting carbon shell is a hard carbon or nongraphitizable carbon. The RF gel is one of the cross-linked polymers which are reportedly prone to becoming a hard carbon after carbonization process.[20]

Electrochemical characterization of Sn-carbon core-shell powder.—Four different samples (Table I) were electrochemically characterized. As well as the Sn-carbon core-shell powder (CSP), the control samples such as a spherical carbon powder (SC), Sn nanoparticles that are not encapsulated (SN), and a mixture of

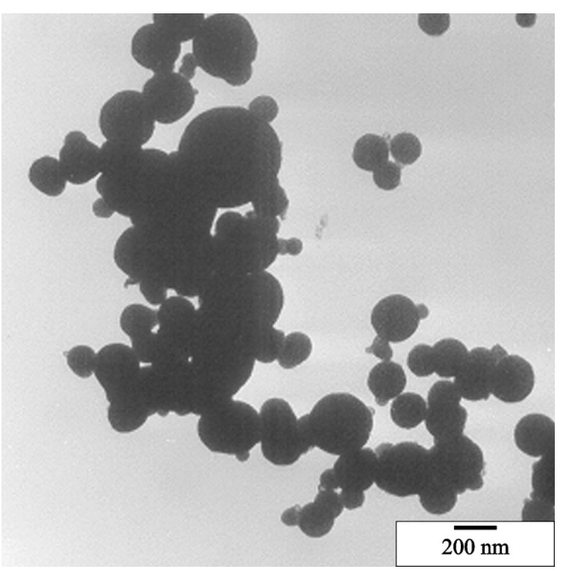

Figure 1. TEM image of Sn nanoparticles used for the preparation of core-shell powder.

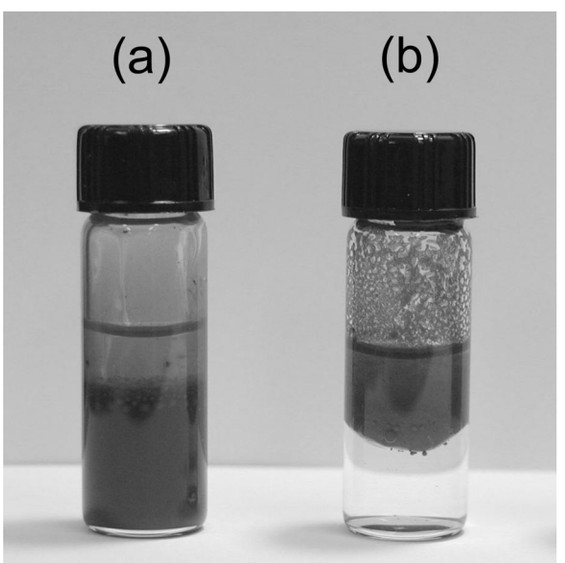

Figure 2. Photographs of (a) the bare Sn nanoparticles and (b) hydrophobized Sn nanoparticles that were dispersed in a mixture of *n*-hexane (upper) and water (lower).

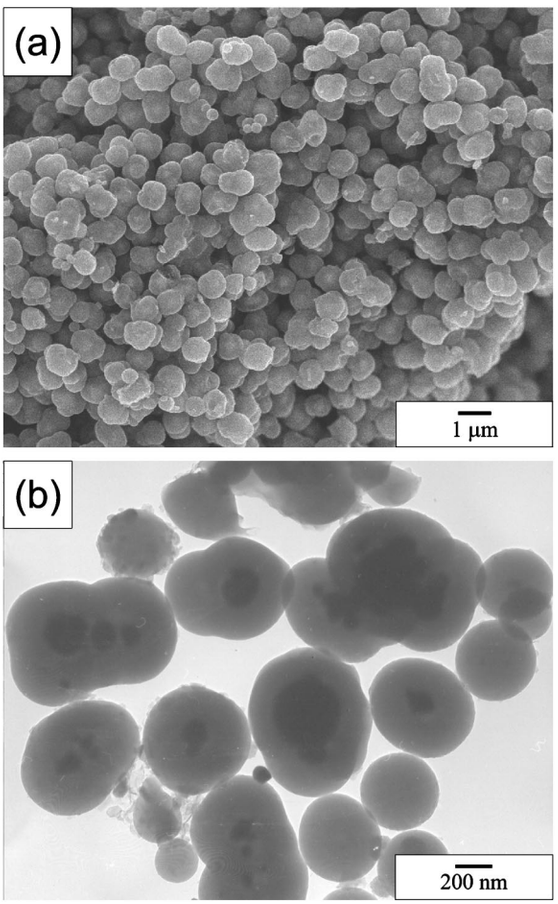

Figure 3. (a) FE-SEM, and (b) TEM images of a Sn-carbon core-shell powder.

spherical carbon and Sn nanoparticles (MIX) are included. SC was prepared using the same process as CSP except that the Sn nanoparticles were not added.

Typical charge-discharge voltage curves of CSP are given in Fig. 5. Plateaus around 0.4-0.8 V range correspond to the electrochemical alloying/dealloying reaction between Li^+ ion and Sn.[21] The background voltage profiles that are associated with the Li^+ insertion/removal into/from carbon also appear, where the different voltage slopes at three different potential regions (0-0.12 V, 0.12-0.8 V, and above 0.8 V) in the discharge profiles are recognized. This reflects the presence of three different Li^+ storage sites in carbon shell, which is one of the characteristic features found in hard carbons that are prepared from cross-linked polymeric precursors or isotropic pitches.[20,22-25] In the first cycle, the charging and discharging capacities are 773 and 424 mAh g^{-1}, respectively, from which a Coulombic efficiency of 55% is calculated. It is well known that hard carbons show a lower Coulombic efficiency compared to graphites. The irreversible capacity of hard carbons at the first cycle is attributed to the solid electrolyte interface (SEI) formation, the degree of which is proportional to the surface area of carbon and the irreversible storage (trapping) of Li^+ ions at void or cavity sites that are highly populated in this type of carbons.[26-29]

Table I. Description of the samples used for the electrochemical characterization.

Sample	Description	Sn content/wt %
SC	Spherical carbon	0
SN	Sn nanoparticles	100
MIX	Mixture of spherical carbon and Sn nanoparticles	20[a]
CSP	Sn-carbon core-shell powder	20[a]

[a] Determined from TGA profiles.

Figure 6 shows the differential charging capacity profiles in the first two cycles for the samples listed in Table I. If a peak in the first cycle disappears in the second cycle, it can be regarded as an irreversible one. The peak near 0.0 V observed with the carbon-containing electrodes (SC, MIX, and CSP) corresponds to the reversible reaction of carbon shell with Li^+ ion, whereas two distinguishable peaks at around 0.65 and 0.40 V observed with the Sn-containing electrodes (SN, MIX, and CSP) correspond to the alloying reactions of Sn core. In addition to these reversible peaks, several irreversible peaks are recognized above 0.7 V. In the profile of SC, two irreversible peaks (#) at 0.80 and 1.25 V are located that are associated with the electrolyte decomposition on carbon surface. In the profile of SN, however, the irreversible peaks (*) are found at different potentials, 1.05 and 1.55 V, which are also related to the catalytic decomposition of electrolyte on Sn surface.[10,30-32] In the profile of MIX, all the irreversible peaks corresponding to carbon and Sn are present together. In the profiles of CSP, however, the irreversible peaks from the Sn component (*) at 1.05 and 1.55 V are

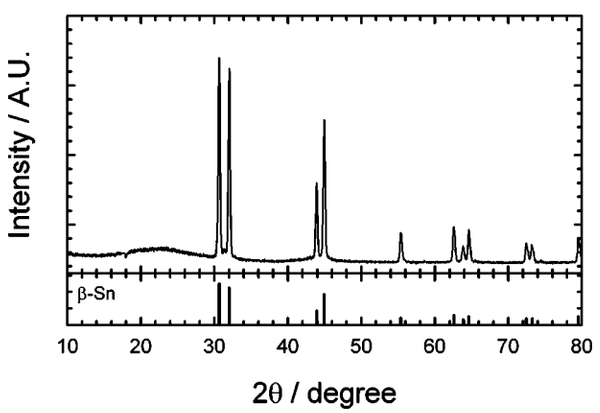

Figure 4. XRD pattern of the Sn-carbon core-shell powder. The reference peaks for β-Sn are drawn based on the data in JCPDS no. 04-0673 (λ = 1.54056 Å).

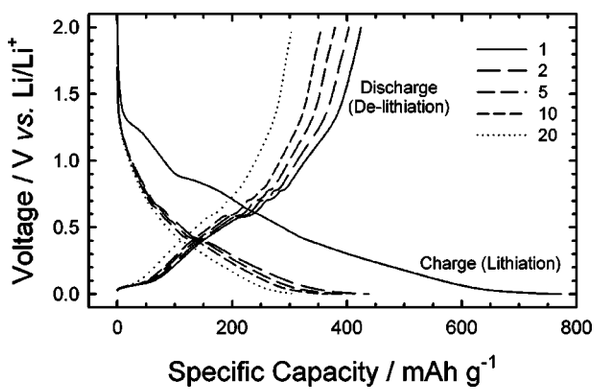

Figure 5. Charge/discharge (lithiation/delithiation or alloying/dealloying) voltage profiles of Sn-carbon core-shell powder at the rate of 40 mA g^{-1} cycled between 0.0 and 2.0 V (vs Li/Li^+). The profiles at the 1st, 2nd, 5th, 10th, and 20th cycles are given.

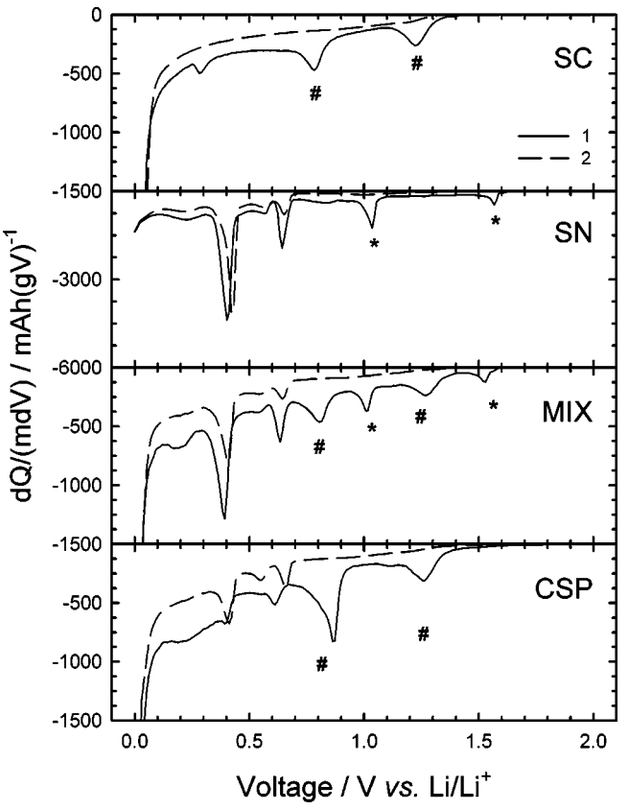

Figure 6. Differential charging capacity profiles during the first two cycles for SC, SN, MIX, and CSP electrodes (Table I). Symbols of "#" and "∗" represent the irreversible peaks corresponding to carbon and Sn, respectively.

not found, implying that the Sn metal surface in CSP electrode is not exposed to the electrolyte. This confirms that the Sn nanoparticles are well encapsulated by the carbon shell.

Figure 7 compares the cycle performance of CSP to that of the control samples (SN and MIX). The results are summarized in Table II along with some initial performance data. The capacity retention of MIX is better than that of SN, while the first discharging capacity is less. It suggests that the spherical carbon in MIX can serve as a

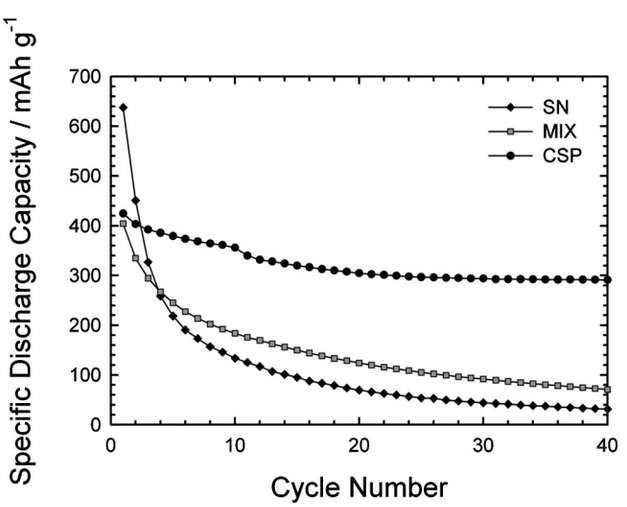

Figure 7. The specific discharge capacity of SN, MIX, and CSP electrodes according to cycle number.

Table II. Summary of electrochemical performance of the samples.

Sample	First discharging specific capacity/mAh g^{-1}	Capacity retained at cycle/%		
		10th	20th	40th
SN	638	21	11	3
MIX	404	46	31	10
CSP	424	84	72	69

buffering phase accommodating the volume expansion of Sn. Despite the same Sn contents (20 wt %) in MIX and CSP, the cyclability of CSP is considerably better than that of MIX, suggesting the core-shell structure provides a significant advantage in maintaining the structural integrity of electrodes. It is believed that the core-shell structure not only prohibits the aggregation of Sn particles but also provides an intimate electrical contact to Sn particles to maintain the conduction path between Sn core and carbon shell. In order to confirm if the latter favorable feature is really prevails, the GITT was used to keep track of the polarization variation while the electrodes were being charged or discharged. Figure 8a shows the overall transient voltage profile of CSP in the second cycle. A typical voltage transient upon a single current pulse cycle during charging is represented in the inset. When the current pulse is applied during charging, voltage increases to reach the closed circuit voltage (CCV) due to the ohmic and charge-transfer resistance.[33] Upon a turn-off of current pulse, voltage drops to reach a quasi-equilibrium value (QOCV). Figure 8b shows the variation of polarization for MIX, the difference between CCV and QOCV in each voltage transient, where two features are immediately apparent. First, the polarization becomes smaller at more negative potentials in the charging period, whereas it steadily increases at more positive potentials in the discharging period. A similar observation was made in the Si composite electrodes where Si powder, carbon additive, and polymeric binder were loaded.[33] The evolution of polarization with cycling can be rationalized as follows. Sn particles are expanded upon charging as a result of alloying reaction with Li^+ ions, which leads to a swelling of the electrode layer. In the forthcoming discharging period, Sn particles are contracted as a result of dealloying reaction, but the electrode layer remains swollen because the electrode layer is not elastic. The net result after a cycle is a loosening or weakening of the electrical contact between Sn and carbon particles, which leads to an increase in polarization. A slight decrease in polarization in the charging period is due to a better contact made between Sn and carbon particles as a result of volume expansion in Sn particles. The second feature observed in Fig. 8b is the ever-increasing polarization with cycling. This must result from a gradual electrode degradation caused by the breakdown of conductive network, which also accounts for a poor cycle performance for MIX (Fig. 7). The polarization behavior of CSP is totally different from that for MIX (Fig. 8c). The anode polarization increases only slightly in the discharging period. Moreover, the polarization does not vary significantly even after repeated cell cycling. It is thus safe to say that the electrical contact between Sn core and carbon shell is well maintained even after a severe volume change in Sn core.

Figure 9 represents the differential discharging capacity profiles for the samples listed in Table II. Four separable peaks in the range 0.4 to 0.8 V correspond to the dealloying reaction of Sn, whereas a broad peak at 0.05 V and a weak peak near 1.2 V correspond to the Li^+ removal from the carbon. Counting only the discharge capacity delivered by Sn, it is apparent that the capacity retention of core-shell powder (CSP) electrode is better than that of either bare Sn (SN) or mixture (MIX) electrode. In the case of CSP electrode, the intensity of four peaks corresponding to the dealloying of Sn is still significant even after 20 cycles (Fig. 9), whereas those in SN or MIX electrodes decay rapidly (Fig. 9). Even in the CSP electrode, however, a slow but steady capacity loss in both Sn and carbon

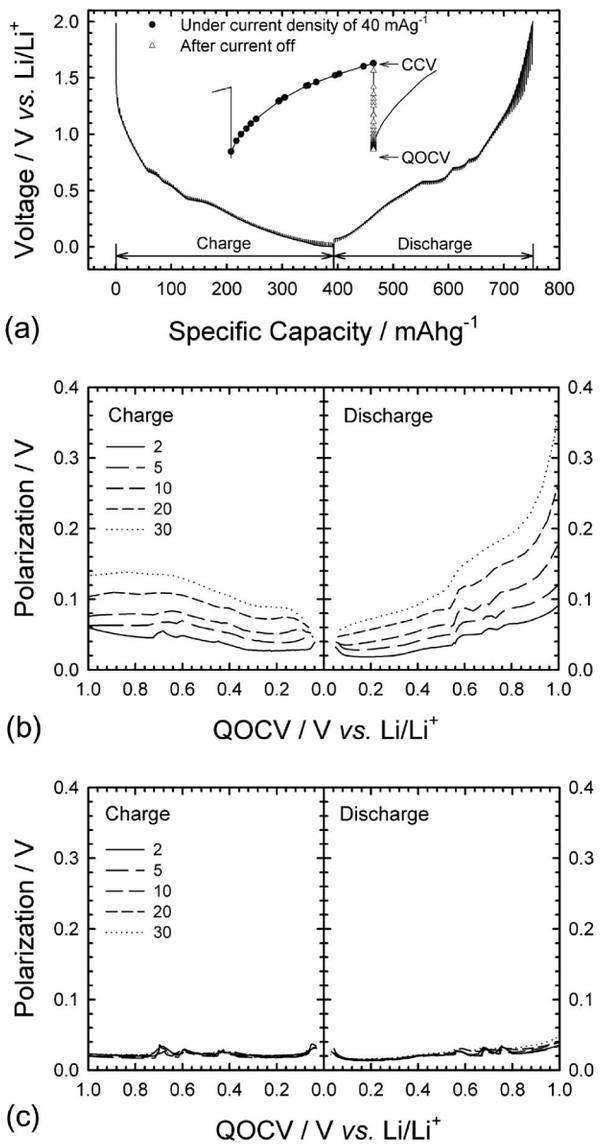

Figure 8. (a) Transient voltage profile obtained with the CSP electrode in the second cycle. A typical voltage transient in a single current pulse cycle during charging is enclosed as inset. (b) Potential-dependent polarization behavior of the MIX electrode at the 2nd, 5th, 10th, 20th, and 30th cycles. (c) Potential-dependent polarization for the CSP electrode.

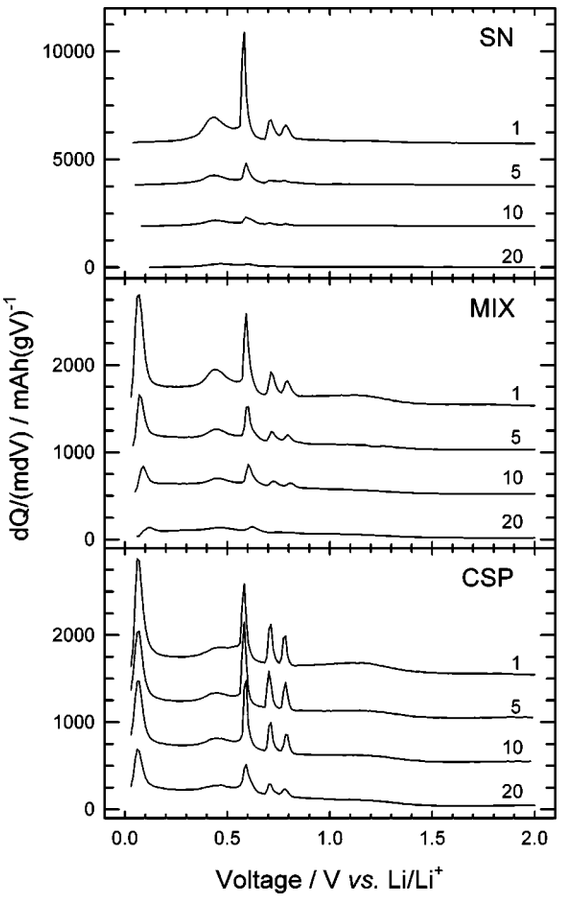

Figure 9. Differential discharging capacity profiles taken with the electrodes. Profiles in the 1st, 5th, 10th, and 20th cycles are given.

components is unavoidable, as indicated by the diminution of all the peaks in Fig. 9 upon cycling. In order to examine the cause of capacity decay in the CSP electrode, the particle morphology after cycles has been examined. Figure 10a and b are the TEM images of selected particle taken from the CSP electrode at the end of the first charge and the first discharge, respectively. It is immediately noticed that the Sn cores have not yet been aggregated, well protected by the carbon shell. Figure 10a shows that a part of the carbon shell has been broken, which may be the result of volume expansion in Sn core upon Li^+ insertion. Moreover, a significant volume expansion of Sn particle is found. Figure 10b shows the void between Sn and carbon, which might have been generated by the contraction of Sn core as Li^+ is extracted. The evolution of void space and crack may explain the slight but apparent capacity loss encountered in both Sn and carbon components in this core-shell structured electrode.

We believe that the cycle life can be further improved by optimizing the design of core-shell structure. For example, either an employment of even smaller metal nanoparticles or replacement of Sn with alloys such as SnSb, or both, would provide a better cyclability. Accordingly, our future work will focus on controlling the size and the composition of metal core, carbon shell thickness, and so forth.

Conclusion

Using an RF microemulsion polymerization performed in the presence of hydrophobized Sn nanoparticles, Sn-carbon core-shell powder was synthesized. The encapsulation of Sn core with carbon shell was confirmed both by TEM images and by the absence of irreversible peaks in the differential capacity profiles. The Sn-carbon core-shell structured powder showed an improved cycle performance compared to the physical mixture comprising Sn and carbon. The enhanced cycle performance is believed to be due to the inhibition of aggregation between Sn particles as well as the intimate contact between Sn core and carbon shell. The latter favorable feature was ascertained by the GITT results. The differential discharging capacity profiles illustrate that the capacity decays in both Sn and carbon components. The TEM images of Sn-carbon core-shell powder after cycling suggest that the cracks in carbon shell and the voids between Sn and carbon are developed due to the volume change of Sn core, which can explain a slow but obvious capacity decay in this electrode.

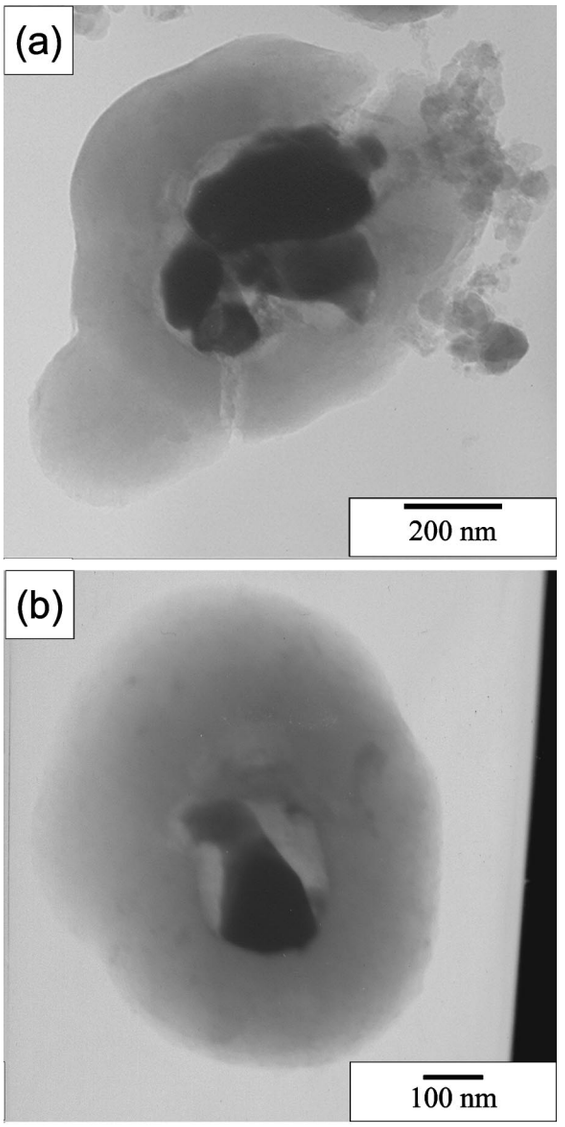

Figure 10. TEM images of Sn-carbon core-shell particle collected at the end of (a) the first charge; and (b) the first discharge.

Acknowledgment

This work was supported by KOSEF through the Research Center for Energy Conversion and Storage and also by the Division of Advanced Batteries in NGE Program (project no. 10016446).

References

1. Y. Idota, T. Kubota, A. Matsufuji, Y. Maekawa, and T. Miyasaka, *Science*, **276**, 1395 (1997).
2. M. Winter, J. O. Besenhard, M. E. Spahr, and P. Novák, *Adv. Mater. (Weinheim, Ger.)*, **10**, 725 (1998).
3. M. Winter and J. O. Besenhard, *Electrochim. Acta*, **45**, 31 (1999).
4. L. Y. Beaulieu, K. W. Eberman, R. L. Turner, L. J. Krause, and J. R. Dahn, *Electrochem. Solid-State Lett.*, **4**, A137 (2001).
5. J. Yang, M. Winter, and J. O. Besenhard, *Solid State Ionics*, **90**, 281 (1996).
6. H. Li, Q. Wang, L. Shi, L. Chen, and X. Huang, *Chem. Mater.*, **14**, 103 (2002).
7. M. Wachtler, M. Winter, and J. O. Besenhard, *J. Power Sources*, **105**, 151 (2002).
8. K. D. Kepler, J. T. Vaughey, and M. M. Thackeray, *Electrochem. Solid-State Lett.*, **2**, 307 (1999).
9. L. M. L. Fransson, J. T. Vaughey, K. Edström, and M. M. Thackeray, *J. Electrochem. Soc.*, **150**, A86 (2003).
10. N. Tamura, R. Ohshita, M. Fujimoto, S. Fujitani, M. Kamino, and I. Yonezu, *J. Power Sources*, **107**, 48 (2002).
11. J. Yin, M. Wada, S. Tanase, and T. Sakai, *J. Electrochem. Soc.*, **151**, A583 (2004).
12. A. Ulus, Y. Rosenberg, L. Burstein, and E. Peled, *J. Electrochem. Soc.*, **149**, A635 (2002).
13. I. S. Kim, G. E. Blomgren, and P. N. Kumta, *Electrochem. Solid-State Lett.*, **7**, A44 (2004).
14. K. T. Lee, Y. S. Jung, and S. M. Oh, *J. Am. Chem. Soc.*, **125**, 5652 (2003).
15. J. Yang, M. Wachtler, M. Winter, and J. O. Besenhard, *Electrochem. Solid-State Lett.*, **2**, 161 (1999).
16. I. A. Courtney, W. R. McKinnon, and J. R. Dahn, *J. Electrochem. Soc.*, **146**, 59 (1999).
17. H. Li, L. Shi, W. Lu, X. Huang, and L. Chen, *J. Electrochem. Soc.*, **148**, A915 (2001).
18. L. Quaroni and G. Chumanov, *J. Am. Chem. Soc.*, **121**, 10642 (1999).
19. X. Xu, G. Friedman, K. D. Humfeld, S. A. Majetich, and S. A. Asher, *Adv. Mater. (Weinheim, Ger.)*, **13**, 1681 (2001).
20. J. R. Dahn, T. Zheng, Y. Liu, and J. S. Xue, *Science*, **270**, 590 (1995).
21. I. A. Courtney, J. S. Tse, O. Mao, J. Hafner, and J. R. Dahn, *Phys. Rev. B*, **58**, 15583 (1998).
22. Y. Liu, J. S. Xue, T. Zheng, and J. R. Dahn, *Carbon*, **34**, 193 (1996).
23. N. Takami, A. Satoh, T. Ohsaki, M. Kanda, *Electrochim. Acta*, **42**, 2537 (1997).
24. C. W. Park, S. H. Yoon, S. I. Lee, and S. M. Oh, *Carbon*, **38**, 995 (2000).
25. O. J. Kwon, Y. S. Jung, J. H. Kim, and S. M. Oh, *J. Power Sources*, **125**, 221 (2004).
26. A. N. Dey and B. P. Sullivan, *J. Electrochem. Soc.*, **117**, 222 (1970).
27. D. Aurbach, Y. Ein-Eli, O. Chusid, Y. Cameli, M. Babai, and Y. Yamin, *J. Electrochem. Soc.*, **141**, 603 (1994).
28. J. O. Besenhard, M. Winter, J. Yang, and W. Biberacher, *J. Power Sources*, **54**, 228 (1995).
29. K. Guerin, A. Fevrier-Bouvier, S. Flandrois, B. Simon, and F. Biensan, *Electrochim. Acta*, **45**, 1607 (2000).
30. L. Y. Beaulieu, S. D. Beattie, T. D. Hatchard, and J. R. Dahn, *J. Electrochem. Soc.*, **150**, A419 (2003).
31. S. D. Beattie, T. Hatchard, A. Bonakdarpour, K. C. Hewitt, and J. R. Dahn, *J. Electrochem. Soc.*, **150**, A701 (2003).
32. N. Pereira, L. C. Klein, and G. G. Amatucci, *Solid State Ionics*, **167**, 29 (2004).
33. J. H. Ryu, J. W. Kim, Y. E. Sung, and S. M. Oh, *Electrochem. Solid-State Lett.*, **7**, A306 (2004).